DOI: 10.19884/j.1672-5220.202402005

Preparation and Properties of Self-Crimping Polyamide-Based Side-by-Side Bicomponent Elastic Fibers

WU Yuhao[1], LANG Jiarui[1], ZHANG Shengming[1], LIU Jin[1], WANG Chaosheng[1*], WANG Huaping[1], JI Peng[2*]

1. State Key Laboratory for Modification of Chemical Fibers and Polymer Materials, College of Materials Science and Engineering, Donghua University, Shanghai 201620, China
2. Innovation Center for Textile Science and Technology, Donghua University, Shanghai 201620, China

Abstract: Side-by-side bicomponent fibers have a spring-like three-dimensional spiral crimp structure and are widely used in elastic fabric. The difference in thermal shrinkage between different polymers can produce an unbalanced stress during the cooling process, and this unbalanced stress can be exploited to prepare naturally crimped fibers by spinning design. In this work, different types of polyamides (PAs) were selected for fabrication of the PA-based side-by-side bicomponent elastic fibers using melt spinning, and the structure development and performance of such bicomponent elastic fibers were studied. Meanwhile, thermoplastic PA elastomer (TPAE) with intrinsic elasticity was also used as one of the comparative materials. The block structure of the PA segment and the polyether segment in the TPAE molecule is the key to providing thermal shrinkage differences and forming a good interface structure. As a result, the crimp ratio of PA6/TPAE bicomponent elastic fiber is 7.23%, which is better than that of the currently commercialized T400 fiber (6.72%). The excellent crimp performance of PA6/TPAE bicomponent elastic fibers comes from the asymmetric distribution of the stress along the radial direction of the fibers during the cooling process, which is caused by the difference in thermal shrinkage between PA6 and TPAE. In addition, the crimp formability of the PA-based bicomponent elastic fibers could be improved by expanding the shrinkage stress through wet-heat treatment. The crimp ratio of PA6/TPAE bicomponent elastic fibers reaches the maximum (33.08%) after treatment at 100 ℃. At the same time, the fabric made of PA6/TPAE bicomponent elastic fibers has the excellent air and water vapor permeability, with an air permeability of 272.76 mm/s and a water vapor transmission rate of 406.71 g/(m^2·h).

Key words: bicomponent fiber; polyamide (PA) fiber; self-crimping; crimp formation ability; melt spinning

CLC number: TQ342+.94 **Document code**: A

Article ID: 1672-5220(2024)06-0569-13

Open Science Identity (OSID)

0 Introduction

Elastic fibers, as a fiber category with high elongation, high elasticity and good comfort, are widely used in apparel, home textiles and other fields[1-4]. Elastic fibers can be divided into intrinsic elastic fibers and morphological elastic fibers according to the elastic mechanism[5]. Intrinsic elastic fibers are block copolymers formed by alternately connecting soft and hard segments. The soft segments can undergo large deformation under minor stresses, while the hard segments serve as physical cross-linking points to prevent the slippage of macromolecular segments[6-8], such as polyurethane fiber and polyolefin fiber. Morphological elastic fibers are due to the special macromolecular structure of the polymer, which obtains elasticity through internal crystalline transformation or changes in molecular conformation[2,9], such as polytrimethylene terephthalate (PTT) fibers and polybutylene terephthalate (PBT) fibers. In addition to intrinsic elastic fibers, side-by-side bicomponent melt spinning is a novel processing technology that can be used to prepare elastic fibers with a wool crimp structure. Compared to intrinsic elastic fibers, side-by-side bicomponent elastic fibers are characterized by flexible and designable properties with freely selectable polymer compositions[10]. The crimp structure brought by structural changes can directly determine the elastic properties of the fibers[11]. Meanwhile, the side-by-side bicomponent elastic fibers can be directly used in fabric manufacturing without preparation into yarns blending with other fibers. Therefore, side-by-side bicomponent elastic fibers with a designable crimp structure are gradually receiving considerable attention.

According to the different distribution of the two component materials in the fibers, bicomponent elastic

Received date: 2024-02-21

Foundation items: Fundamental Research Funds for the Central Universities of China (No. 2232022D-10); Open Fund of State Key Laboratory of Biobased Fiber Manufacturing Technology, China (No. SKL202306)

* Correspondence should be addressed to JI Peng, email: jipeng@dhu.edu.cn; WANG Chaosheng, email: cswang@dhu.edu.cn

Citation: WU Y H, LANG J R, ZHANG S M, et al. Preparation and properties of self-crimping polyamide-based side-by-side bicomponent elastic fibers[J]. *Journal of Donghua University (English Edition)*, 2024, 41(6): 569-581.

fibers can be divided into sheath-core type, side-by-side type and matrix fibril type[11-12]. The side-by-side bicomponent elastic fiber is based on the difference in thermal shrinkage properties of the components, causing the fiber to bend away from the fiber axis, and finally presents a permanent three-dimensional spiral crimp[13-14]. This crimp structure has good stability and elasticity, which gives the fabric better elasticity and bulkiness[15-16]. The main factors that affect the crimp properties of side-by-side bicomponent elastic fibers are the distribution form of each component and the kind of two components. This distribution form determines the radial stress distribution of the fiber, thereby affecting the crimp performance[10,17-19]. The dumbbell-shaped cross-section exhibits the best crimp and elastic properties compared to the gourd-shaped and the round-shaped[20]. The difference in heat shrinkage characteristics between the two components is equally important in influencing the fiber crimp structure. Yu et al.[13] prepared a series of polylactic acid (PLA)/PTT side-by-side bicomponent fibers and pointed out that the main reason for fiber curling was the structural difference resulting in an uneven fiber force during cooling. Therefore, the crimp forming of fibers can be effectively improved by expanding the shrinkage stress difference between the two components. In addition to the material properties and the processing method, heat treatment after fiber forming is also an important method to promote crimp forming[15]. During the heat treatment, the difference in movement of molecular chains in the amorphous region between the two components will promote the formation of a three-dimensional crimp structure.

As one of the earliest industrialized synthetic fibers, polyamide (PA) fibers have excellent strength, wear resistance, elasticity and moisture absorption[21-23]. However, compared with the large number of studies on polyester-based side-by-side bicomponent fibers, there are very few related studies on PA-based side-by-side bicomponent fibers, mainly because of the poor interfacial compatibility between PA and other components[24-25]. PA-based polymers are difficult to meet the spinning requirements, which makes PA-based side-by-side bicomponent fibers research standstill. With the development of PA synthesis research, thermoplastic PA elastomer (TPAE) has been successfully synthesized as a block copolymer with intrinsic elasticity[26-28]. The PA chains as hard segments ensure a stable interfacial structure with other PA components. However, the structure and properties of the side-by-side bicomponent fibers with TPAE as a component have not been reported so far.

Based on the above research background, this work focuses on the crimp formability of PA-based side-by-side bicomponent elastic fibers prepared by melt spinning. The effects of viscosity and structural differences on the fiber crimp structure are investigated using PAs (with different types and viscosities) and TPAE as the components of the side-by-side bicomponent elastic fibers. Further, their application properties are compared with those of commercial T400 fibers. PA-based side-by-side bicomponent elastic fibers are expected to meet the requirements of elastic products with higher skin-friendly properties. We hope this work can provide some useful references for the development of new PA-based bicomponent elastic fibers.

1 Materials and Methods

1.1 Materials

PA6 with relative viscosity of 2.40 was purchased from Poly Plastic Masterbatch (Suzhou) Co., Ltd., China. PA6 with relative viscosity of 2.85 and 3.40 were purchased from Baling Petrochemical Co., Ltd., China. These samples were denoted as PA6-2.40, PA6-2.85 and PA6-3.40, respectively. PA66 with relative viscosity of 2.40 was purchased from Zhejiang Huafon New Materials Co., Ltd., China. T400 fiber (PTT/polyethylene terephthalate side-by-side bicomponent elastic fiber, 55 dtex, 36 F) was supplied by Hengyi Petrochemical Co., Ltd., China. TPAE was purchased from Beijing Risun Science and Technologies Co., Ltd., China.

The chemical structure and ^{1}H NMR of TPAE are shown in Fig. 1, in which δ denotes the chemical shift. The deuterated trifluoroacetic acid (TFA-d) is used as the solvent of TPAE for ^{1}H NMR testing. The mass fraction of PA hard segments in TPAE is calculated by ^{1}H NMR[29-30] to be 65.5%.

In order to provide a reference for the melt spinning temperature, the thermal properties of the individual PA components were measured through the differential thermal analysis test and the melt viscosity of individual component was measured using a capillary rheometer (RH2000, Malvern, UK). The thermal performance parameters are shown in Table 1, and the non-Newtonian and structural viscosity indices of the individual component melts at different temperatures are listed in Table 2.

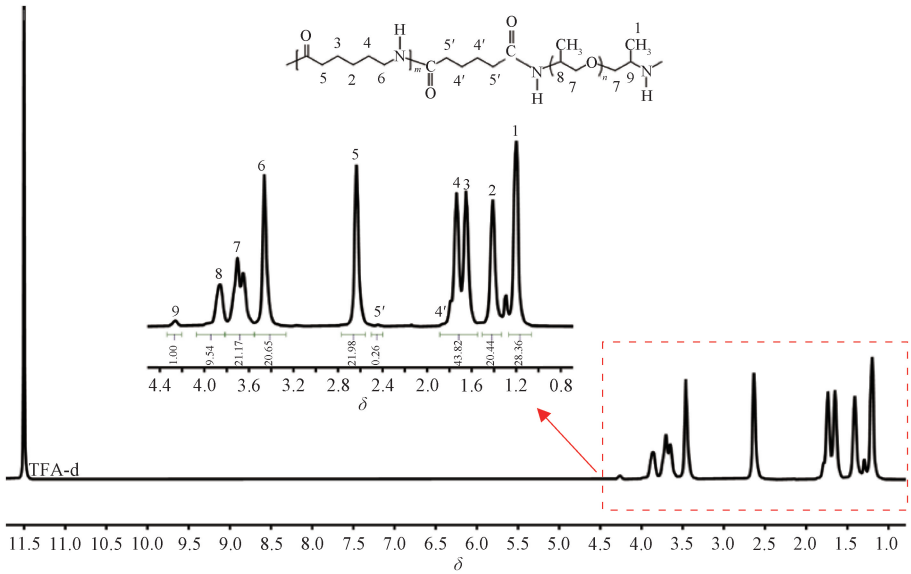

Fig. 1 ^{1}H NMR spectrum and chemical structure of TPAE

Table 1 Thermal performance parameters of individual PA component

Sample	T_c/℃	ΔH_c/(J/g)	T_m/℃	ΔH_m/(J/g)	$t_{1/2}$/min
PA6-2. 40	163. 73	60. 47	220. 72	64. 15	1. 65
PA6-2. 85	165. 84	58. 96	220. 92	54. 66	1. 58
PA6-3. 40	165. 58	54. 47	220. 50	51. 00	1. 54
PA66	212. 51	65. 28	258. 70	63. 84	1. 01
TPAE	139. 76	37. 90	206. 58	36. 98	1. 25

Note: $t_{1/2}$ is the half-crystallization time.

Table 2 Non-Newtonian and structural viscosity indices of the individual component melts at different temperatures

Sample	Temperature/℃	Non-Newtonian index n	Structural viscosity index $\Delta\eta$
	260	0. 48	1. 21
PA6-2. 40	265	0. 57	0. 99
	270	0. 68	1. 06
	260	0. 41	1. 35
PA6-2. 85	265	0. 43	1. 31
	270	0. 46	1. 38
	265	0. 31	1. 69
PA6-3. 40	270	0. 32	1. 65
	275	0. 33	1. 81
	280	0. 69	0. 70
PA66	285	0. 71	0. 66
	290	0. 72	0. 68
	275	0. 57	1. 14
TPAE	280	0. 64	1. 43
	285	0. 73	1. 56

1. 2 Preparation of PA-based side-by-side bicomponent elastic fibers and fabrics

The PA-based side-by-side bicomponent elastic fibers were obtained by using a bicomponent melt-spinning machine (ABEϕ25×2, Abe Machinery Co., Ltd., Japan). Figure 2 shows a schematic diagram of the spinning process. A spinneret with 36 holes was selected, the shape of each hole was dumbbell-shape, and the spinning speed was 1 000 m/min. The combination of two different components in a bicomponent fiber is shown in Table 3. Five different PA-based side-by-side bicomponent elastic fibers were denoted as PA6-2. 40/PA6-3. 40, PA6-2. 40/PA66, PA6-2. 85/PA66, PA6-3. 40/PA66 and PA6-2. 40/TPAE, respectively. The spinning parameters were determined by characterizing the thermal and rheological properties of the raw materials. The specific parameters are shown in Table 3, and the obtained fibers are shown in Fig. 3(a). In addition, the obtained fibers were woven into PA-based side-by-side bicomponent fabrics, and the T400 fabric was woven for comparison. The obtained fabrics are shown in Fig. 3(b).

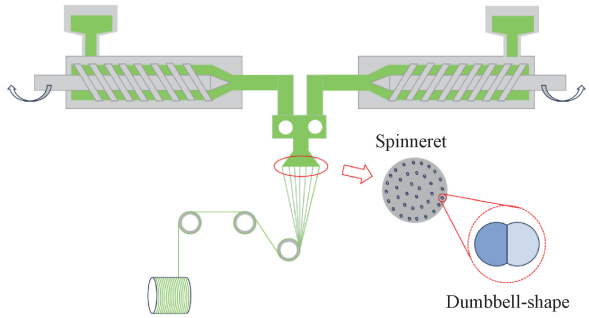

Fig. 2 Schematic diagram of the spinning process

Table 3 Spinning parameters of PA-based side-by-side bicomponent elastic fibers

Sample	Component	Spinning temperature/℃	Spinning speed/(m/min)
PA6-2. 40/PA6-3. 40	PA6-2. 40 PA6-3. 40	265 272	1 000
PA6-2. 40/PA66	PA6-2. 40 PA66	265 285	1 000
PA6-2. 85/PA66	PA6-2. 85 PA66	267 285	1 000
PA6-3. 40/PA66	PA6-3. 40 PA66	272 285	1 000
PA6-2. 40/TPAE	PA6-2. 40 TPAE	270 280	1 000

(a)

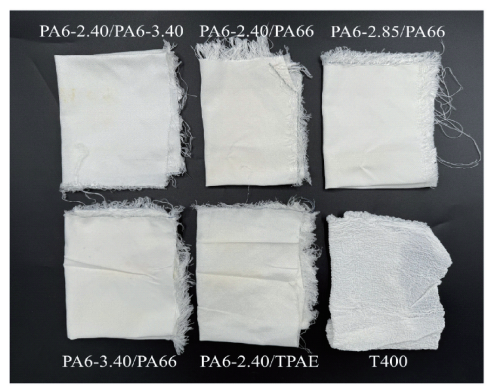

(b)

Fig. 3 Views of PA-based side-by-side bicomponent elastic samples: (a) fibers; (c) fabrics

1.3 Characterization

The cross-section of the PA-based side-by-side bicomponent elastic fibers was observed by a scanning electron microscope (SEM) (S-4800, Hitachi, Japan) with an accelerating voltage of 5 kV. The fibers were treated with liquid nitrogen and gold spray prior to testing. A yarn tensile tester (XL-2, Shanghai Xinxian Instrument Co., Ltd., China) was used to test the mechanical properties. For the tensile test, the tensile speed was 250 mm/min, and the test interval was 250 mm. Each sample was tested 10 times and the average value was taken. For the cyclic tensile test, the PA-based side-by-side bicomponent elastic fibers were repeatedly exposed to consecutive cycles to a constant strain (5%, 10% and 15%) at a constant speed of 100 mm/min. The elastic recovery was measured by observing the residual strain after 10 cycles. The crystal structure and crystallinity were performed on an X-ray diffractometer (D/max-2550 VB, Rigaku, Japan) equipped with a filtered Cu Kα radiation source. The crimp feature was performed on a fiber crimp elasticity tester (XCP-1AN, Shanghai Xinxian Instrument Co., Ltd., China) according to GB/T 14338—2022. The length of the fiber under the action of a light load was measured and recorded as L_0. Then, a heavy load was applied to the fiber, and its length was recorded again as

L_1. The heavy load was maintained for 30 s and then removed to return the clamping distance to the initial value. The light load was applied again after 2 min and the length of the fiber was recorded as L_2. The pre-tension under the light load was 0.002 cN/dtex and that under the heavy load was 0.050 cN/dtex. Each sample was tested five times.

The crimp ratio J is calculated as

$$J = \frac{L_1 - L_0}{L_1} \times 100\%.$$

The crimp elastic ratio J_d is calculated as

$$J_d = \frac{L_1 - L_2}{L_1 - L_0} \times 100\%.$$

The crimp recovery ratio J_w is calculated as

$$J_w = \frac{L_1 - L_2}{L_1} \times 100\%.$$

For the moisture regain test, the PA-based side-by-side bicomponent elastic fibers were dried in a drying oven at 100 ℃ to a constant mass m_0. The fibers were taken out subsequently and kept in a test box at a constant temperature of 20 ℃ and a relative humidity of 65% for 48 h. Then, the mass of the fibers was recorded as m_1. Each fiber was tested in parallel for five groups and the average value was taken. The moisture regain D is calculated as

$$D = \frac{m_1 - m_0}{m_0} \times 100\%.$$

The determination of the air permeability of the fabric was conducted on a fabric air permeability tester (YG461E, Wenzhou Fangyuan Instrument Co., Ltd., China). The area of the fabric sample was selected as 20 cm^2. The air flow to make the fabric on both sides of the pressure drop was adjusted to close to 100 Pa. The air flow rate was recorded when the pressure drop was stabilized. The water vapor permeance of the fabric was tested according to GB/T 12704.1—2009. The fabric was placed on the moisture permeable cup containing desiccant, and then the cup with the fabric was kept in a test box at a temperature of 38 ℃ and a relative humidity of 90% for 1 h. Then the cup with the fabric was taken out and kept in a silica gel desiccator at 20 ℃ for 30 min. The mass of the cup with the fabric was recorded. The above steps were repeated and the mass at the second time was recorded. The mass difference between the two recordings was recorded as Δm. At the same time, a blank control group was set up and the mass difference was recorded as $\Delta m'$.

The water vapor transmission rate r_T is calculated as

$$r_T = \frac{\Delta m - \Delta m'}{A \times t},$$

where A is the effective test area; t is the test time.

The water vapor permeance r_p is calculated as

$$r_P = \frac{r_T}{\Delta p} = \frac{r_T}{p_{CB}(R_1 - R_2)},$$

where Δp is the water vapor pressure difference on both sides of the sample; p_{CB} is the saturated vapor pressure of water at experimental temperature; R_1 and R_2 are the relative humidity in the test box and the moisture permeable cup during the test, respectively.

For the dyeing performance test, the fabrics were taken with the same area and dyed with an acid dye in boiling water (exceeding 97 ℃) for 90 min under normal pressure. The mass ratio of the dye to the fabric is 1%.

2 Results and Discussion

2.1 Crimp investigation of PA-based side-by-side bicomponent elastic fibers

2.1.1 Effect of fiber cross-sectional morphologies on crimp structure

Figure 4 shows the cross-section of different PA-based side-by-side bicomponent elastic fibers. The four kinds of fibers composed of PA6 and PA66 show elliptical cross-sections and almost no interface between the components (Figs. 4(a)−4(d)). In contrast, the cross-section of PA6-2.40/TPAE shows an obvious dumbbell-shaped morphology (Fig. 4(e)), which is the same as the shape of the spinneret, and exhibits a clear interface between the components (the region in the red rectangular in Fig. 4(e)). This is due to the complete compatibility of PA6 with different viscosities. PA6 and PA66 have similar molecular chain structures, and hydrogen bonds can be quickly formed on the molecular chains. Based on the principle of "like dissolves like", PA6 and PA66 mix thoroughly after melt extrusion, leading the fiber interfacial structure to disappear upon cooling[31-32]. By contrast, the poor compatibility of the polyether segments in TPAE molecular chains with PA chains leads to a microphase separation between the interfaces[33]. At the same time, the presence of the PA chain segments ensures compatibility with the PA6-2.40 component, resulting in a clear and unseparated interfacial structure.

The relationship between the crimp radius and pitch of side-by-side bicomponent fibers has been analyzed. It is found that when both of the crimp radius and pitch of the fiber tend to be the smallest, the fiber has the highest crimp curvature and the most excellent crimp structure. The crimp radius and pitch are the smallest when the cross-section of the fiber is dumbbell-shaped[20,34]. This means that the crimp structure is positively correlated with the retention of the dumbbell form. Therefore, it can be observed from Fig. 4(e) that PA6-2.40/TPAE has an excellent crimp structure, while other kinds of fibers do not exhibit the crimp structure.

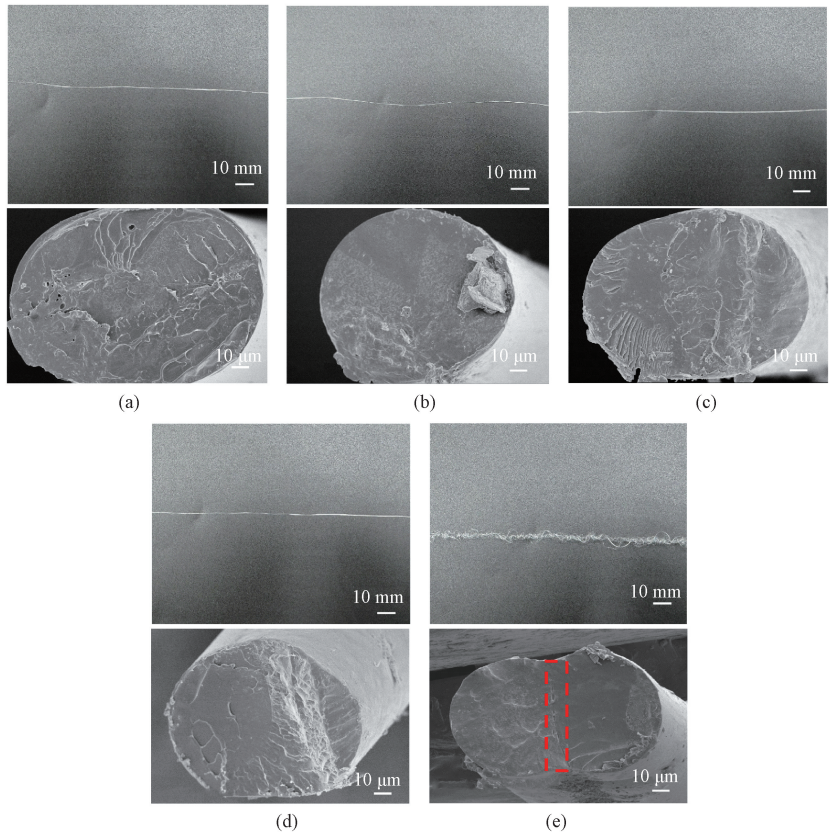

Fig. 4 Morphologies (upper) and cross-sectional SEM images (lower) of different PA-based side-by-side bicomponent elastic fibers: (a) PA6-2.40/PA6-3.40; (b) PA6-2.40/PA66; (c) PA6-2.85/PA66; (d) PA6-3.40/PA66; (e) PA6-2.40/TPAE

2.1.2 Effect of components on crimp properties

In order to investigate the effect of thermal shrinkage differences between components on crimp properties, the PA-based side-by-side bicomponent elastic fibers were heat treated in hot water at 100 ℃ for 25 min. The morphologies before and after wet-heat treatment are shown in Fig. 5.

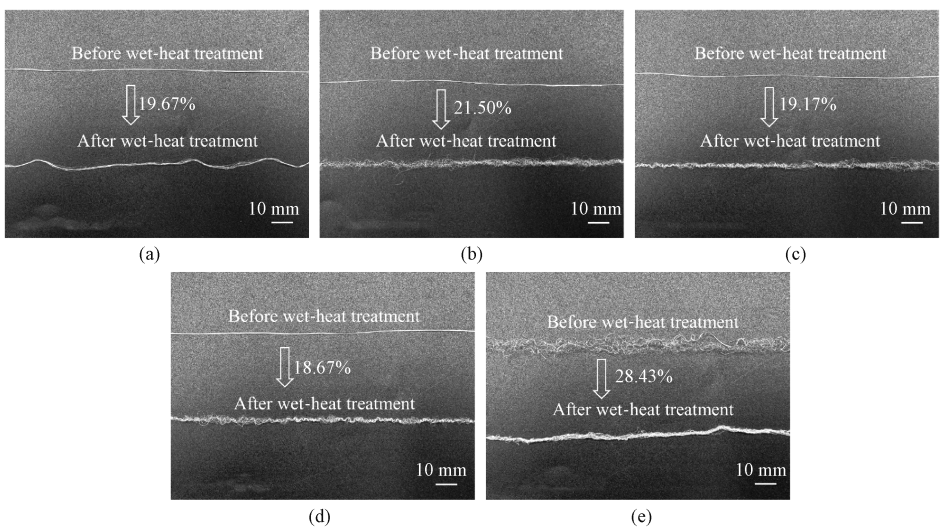

Fig. 5 Morphologies and thermal shrinkage ratios of PA-based side-by-side bicomponent elastic fibers before and after wet-heat treatment: (a) PA6-2.40/PA6-3.40; (b) PA6-2.40/PA66; (c) PA6-2.85/PA66; (d) PA6-3.40/PA66; (e) PA6-2.40/TPAE

The crimp structure of fibers has been significantly improved after wet-heat treatment except for PA6-2.40/PA6-3.40. Figures 6(a) and 6(b) show the crimp properties of PA-based side-by-side bicomponent elastic fibers before and after wet-heat treatment. Before wet-heat treatment, the crimp ratios of PA6-2.40/PA6-3.40, PA6-2.40/PA66, PA6-2.85/PA66, PA6-3.40/PA66 and T400 fibers are 0.98%, 0.75%, 0.78%, 1.09% and 6.72%, respectively. By contrast, the crimp ratio of PA6-2.40/TPAE is 7.23%, even higher than that of the commercial T400 fiber. These results indicate that the formation of the crimp structure of fibers has an obvious dependence on the components. After wet-heat treatment, the crimp ratios of PA6-2.40/PA6-3.40, PA6-2.40/PA66, PA6-2.85/PA66 and PA6-3.40/PA66 increase to 1.32%, 7.44%, 5.99% and 4.97%, respectively. The crimp ratio of PA6-2.40/PA6-3.40 has almost no change, indicating that the difference in viscosity of the same material cannot achieve a difference in thermal shrinkage to form a crimp structure. As the molecular mass of PA6 decreases, the crimp ratio of PA6/PA66 samples increases from 4.97% (PA6-3.49/PA66) to 7.44% (PA6-2.40/PA66). It is worth noting that the crimp ratio of PA6-2.40/TPAE significantly increases to 33.08% after wet-heat treatment, which is much higher than that of other kinds of fibers. It can infer that the improvement in crimp properties after wet-heat treatment mainly results from the unbalanced force between the different PA components, which could be determined by the heat shrinkage performance between the two components. Furthermore, the crimp elastic ratios of all PA bicomponent fibers exceed 90%, indicating a good durability of the crimp structure of fibers.

In order to reveal the mechanism of the formation of the crimp structure, it is necessary to make a detailed comparison of the heat shrinkage behavior. Figure 6(c) shows the thermal shrinkage ratios of fibers in boiling water. PA6-2.40/TPAE has the highest thermal shrinkage ratio of 28.43%. The thermal shrinkage ratios of PA6-2.40/PA6-3.40, PA6-2.40/PA66, PA6-2.85/PA66 and PA6-3.40/PA66 are 19.67%, 21.50%, 19.17% and 18.67%, respectively. All fibers undergo thermal shrinkage, which is a result of the segmental motion in the amorphous region of the polymers[35]. This is because the polyether segments in TPAE are in the amorphous state, which increases the amount of amorphous regions, making TPAE have more segments capable of movement than PA6 and PA66[36]. When the PA6-2.40 component completes the heat shrinkage behavior, the heat shrinkage of the TPAE component is still in progress. At this time, the PA6-2.40 component will hinder the further thermal shrinkage of TPAE, resulting in the unbalanced stresses in the radial direction of the fiber, which leads to the further development of the crimp structure. Similarly, the fiber with PA6 and PA66 as components also develop a crimp structure after wet-heat treatment due to the different thermal shrinkage ratios between PA6 and PA66. However, the PA6-2.40/PA6-3.40 fiber is composed of the same polymer, the thermal shrinkage ratios are close to each other, and thus the crimp structure cannot develop.

Figure 6(c) also shows the sound velocity orientation factor values of the fibers. The sound velocity orientation factor value of PA6-2.40/TPAE is much lower than that of T400 fiber (0.62) and other fibers. Correspondingly, the orientation degree of PA6-2.40/TPAE is lower than that of other fibers, which shows the molecular chains in the fiber are less ordered along the axial direction during the cooling process. This is because the polyether chain segments of the TPAE component are in the amorphous state and can move in the direction of the external force. When the external force is removed, the polyether chain segments in the amorphous region relax and shrink. This is also the reason why PA6-2.40/TPAE can produce a crimp structure during the cooling process, while other fibers cannot produce a crimp structure.

Figure 6(d) and Table 4 show the crystal structure and crystallinity of fibers, respectively. PA6-2.40/TPAE has the lowest crystallinity of 43.29%, indicating that the use of TPAE increases the amorphous area of the fiber. This result also corresponds to the results of the thermal shrinkage of the fiber. In addition, all kinds of fibers show the characteristic peaks of α (200), α (002) and γ (001), corresponding to the α and γ crystal forms of PA6 and PA66, respectively[37-38].

The half-crystallization time values of all components at a cooling rate of 20 ℃/min shown in Table 1 indicate that PA66 has the higher crystallization rate, while TPAE has the lower crystallization rate than PA66. Although the difference in crystallization rates between PA6 and PA66 is higher than that between PA6 and TPAE, only PA6-2.40/TPAE develops a crimp structure. This is mainly because the molecular chain of TPAE is composed of PA segments and polyether segments. During the cooling process, only the PA segment crystallizes, while the polyether segment remains in an amorphous state. The amorphous polyether segment provides more shrinkage stress, causing unbalanced stress between the two components and promoting the development of the crimp structure. The cooling rate during actual processing is much higher than that under the test condition. It can be speculated that the difference in crystallization rate between PA6 and PA66 is too low to cause unbalanced stresses between the two components, thereby failing to produce a crimp structure.

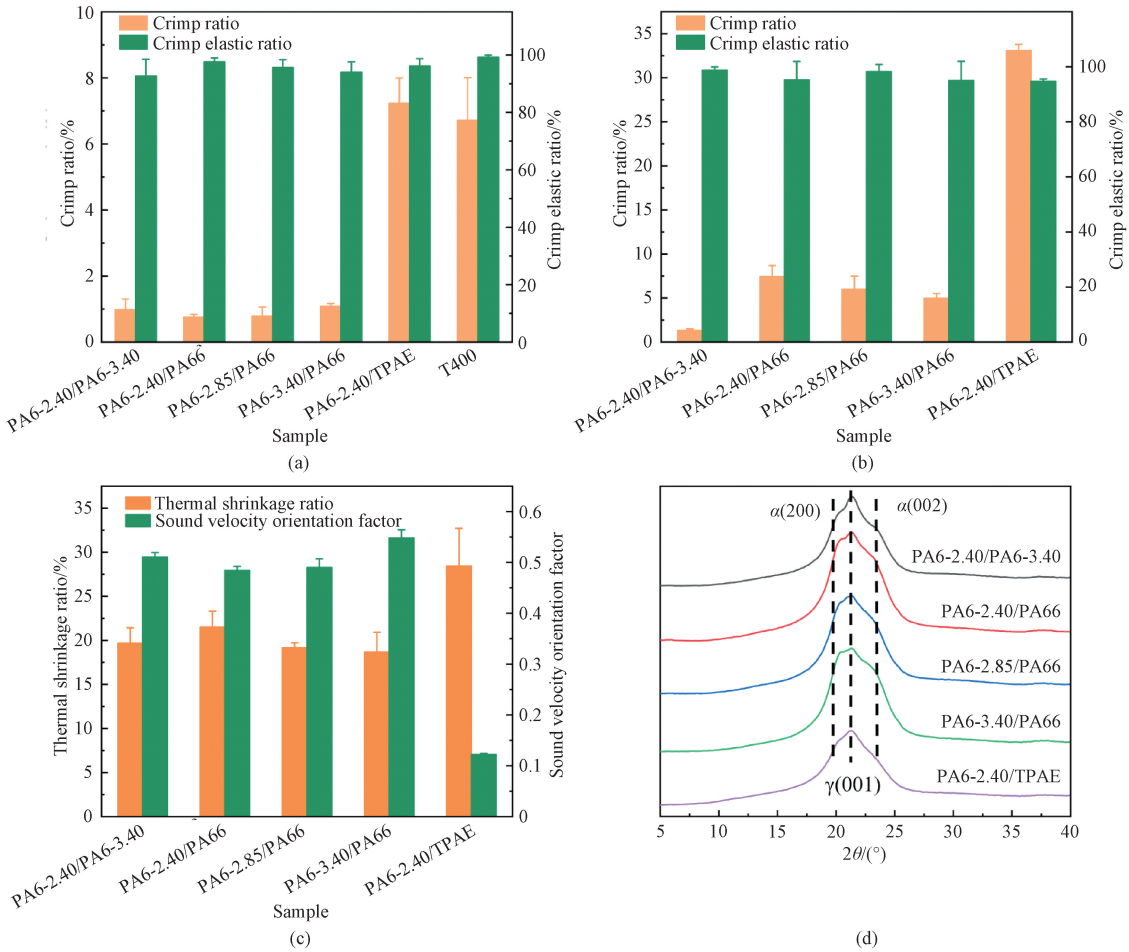

Fig. 6 Properties of PA-based side-by-side bicomponent elastic fibers: (a) crimp properties before wet-heat treatment; (b) crimp properties after wet-heat treatment; (c) thermal shrinkage ratio in boiling water and sound velocity orientation factor; (d) one-dimensional XRD diffraction pattern

Table 4 Crystallinity of PA-based side-by-side bicomponent elastic fibers and dye uptakes of their fabrics

Sample	Crystallinity/%	Dye uptake/%
PA6-2.40/PA6-3.40	48.43	60.01
PA6-2.40/PA66	45.57	84.03
PA6-2.85/PA66	48.05	82.01
PA6-3.40/PA66	50.71	79.54
PA6-2.40/TPAE	43.29	64.90

2.2 Crimping mechanism of PA-based side-by-side bicomponent elastic fibers

The crimping mechanism of PA-based side-by-side bicomponent elastic fibers is shown in Fig. 7. During the spinning cooling process, an obvious interface structure is a necessary condition for the formation of the crimp structure. On this basis, when one component reaches a constant shrinkage value, a rebound force will be generated to hinder the thermal shrinkage of the other component, resulting in asymmetric distribution of the residual stress in the radial direction of the fiber. The excellent compatibility between PA6 and PA66 prevents it from forming an interface structure and therefore cannot form a good crimp structure. In contrast, TPAE as an intrinsic elastomer with PA segments and polyether segments, it can form an excellent dumbbell-shaped cross-section with the PA6 component. At the same time, the present of polyether segments makes the TPAE thermal shrinkage higher than that of PA6, which ultimately leads to asymmetric radial residual stress distribution in the PA6-2.40/TPAE fiber, resulting in an obvious crimp structure. During the wet-heat treatment, the amorphous segments become mobile, resulting in thermal shrinkage of the polymer, and different polymers have different thermal shrinkage ratios. As a result, the fibers with PA6 and PA66 as components show the crimp structure after wet-heat treatment. By contrast, PA6-2.40/PA6-3.40 cannot exhibit the crimp structure even after wet-heat treatment because PA6-2.40 and PA6-3.40 have the close thermal shrinkage ratios. The crimp structure of PA6-2.40/TPAE can also be further developed after wet-heat treatment. Within the same length, PA6-2.40/TPAE has more crimp numbers than other fibers, which implies a better crimp structure.

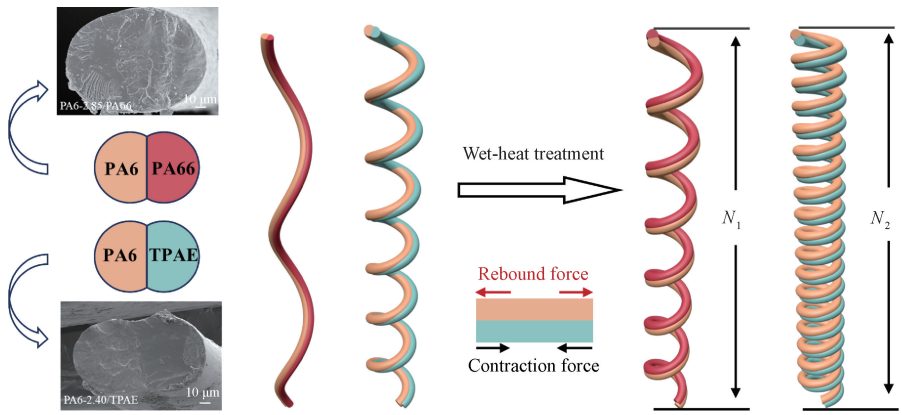

Fig. 7 Mechanism diagram of crimp formation of PA-based side-by-side bicomponent elastic fibers (N_1 and N_2 are the crimp numbers of PA6-2.85/PA66 and PA6-2.40/TPAE within the same length, respectively; $N_1 < N_2$)

2.3 Mechanical properties of PA-based side-by-side bicomponent elastic fibers

The mechanical properties of PA-based side-by-side bicomponent elastic fibers are shown in Figs. 8(a) and 8(b). The breaking strength of all PA-based side-by-side bicomponent elastic fibers composed of PA6 and PA66 exceeds 2.00 cN/dtex. In contrast, PA6-2.40/TPAE exhibits a lower breaking strength (1.50 cN/dtex) and a higher elongation at break (89.66%). The breaking strength of all fibers is lower than that of T400 fiber. Combined with the results of sonic orientation, T400 fiber has the highest degree of orientation and the least amorphous area in the fiber. During the stretching process of the fiber, the movements and breakages of molecular chain segments mainly occur in the amorphous region. For PA6-2.40/TPAE, the introduction of polyether segments in TPAE dereases the hydrogen bond density between PA segments[39], making the TPAE component have a lower modulus and a higher elongation than the PA6 component[40]. Therefore, the amorphous region in the PA6 component is straightened first and undergoes more stress to break, which results in the lower breaking strength of PA6-2.40/TPAE. In contrast, the modulus of the two components of other fibers are close to each other and jointly withstand the stress. Likewise, a large modulus difference causes the two components of the fiber to undergo different stresses during spinning, resulting in unbalanced internal stress, which promotes the generation of fiber crimp structures.

The elastic recovery ratios of PA-based side-by-side bicomponent elastic fibers at different constant elongations are shown in Fig. 8(c). With the increase of constant elongation, the elastic recovery ratios of all fibers decrease after 10 cycles. The reason is that the relative slip between molecular chain segments under large deformation results in permanent deformation (plastic deformation), and becomes more obvious with increasing deformation[41]. Notably, PA6-2.40/TPAE shows the best elastic recovery ratio among all kinds of fibers at 20% constant elongation. For TPAE, the polyether soft segments have a glass transition temperature T_g lower than room temperature and exhibit a highly elastic state, endowing the fiber excellent elastic properties[42]. As a result, the elastic recovery of PA6-2.40/TPAE at 20% constant elongation is higher than that of PA6-2.40/PA66 due to the presence of TPAE.

The moisture regains of PA-based side-by-side bicomponent elastic fibers are shown in Fig. 8(d). PA6-2.40/TPAE fibers have a high moisture regain of 3.37%. The other PA fibers have moisture regains below 3.00%, but they are all much higher than those of T400 fibers. Good moisture absorption can improve the wearing comfort and dyeing ratio. The high moisture regain of PA6-2.40/TPAE fibers is due to the fact that the polyether segment in TPAE is in an amorphous state, making it easier for moisture to enter the fiber.

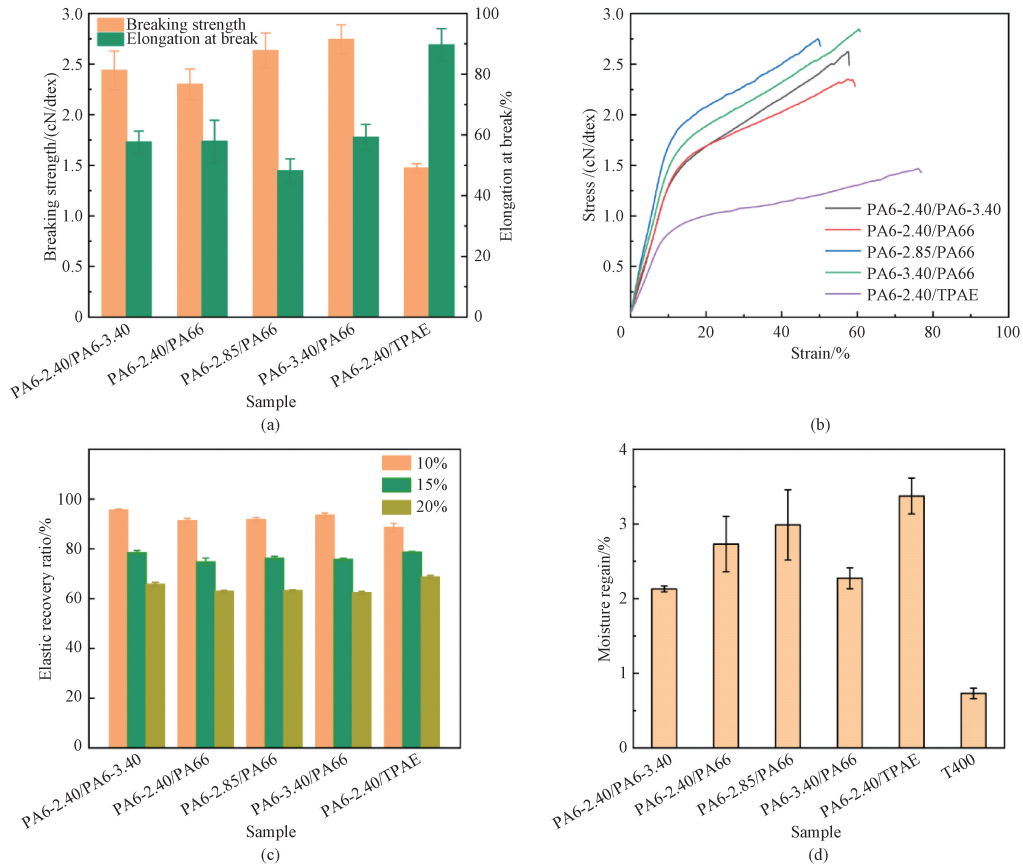

Fig. 8 Physical properties of PA-based side-by-side bicomponent elastic fibers: (a) mechanical properties; (b) tensile testing curves; (c) elastic recovery ratios; (d) moisture regains

2.4 Wear comfort analysis of PA-based side-by-side bicomponent elastic fabrics

The air and water vapor permeabilities are shown in Fig. 9 and Table 5. The PA6-2.40/TPAE fabric exhibits the best air and water vapor permeability, with an air permeability of 272.76 mm/s and a water vapor transmission rate of 406.71 g/(m^2·h), which are 3.93 and 1.71 times that of the T400 fabric (69.43 mm/s and 237.81 g/(m^2·h)), respectively. All PA side-by-side bicomponent elastic fabrics show better air permeability than T400 fabric. It means that the fabrics made of PA-based side-by-side bicomponent elastic fibers have a better wearing comfort.

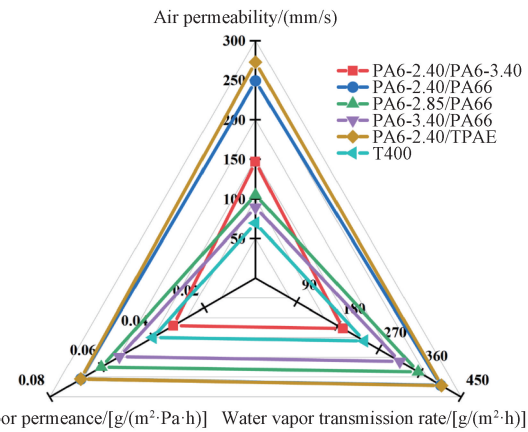

Fig. 9 Air and water vapor permeability of PA-based side-by-side bicomponent elastic fabrics

Table 5 Air and water vapor permeability results of PA-based side-by-side bicomponent elastic fabrics

Sample	Air permeability/(mm/s)	Water vapor permeance/[g/(m^2·Pa·h)]	Water vapor transmission rate/[g/(m^2·h)]
PA6-2.40/PA6-3.40	146.79	0.032	190.81
PA6-2.40/PA66	248.95	0.068	404.95
PA6-2.85/PA66	104.99	0.060	355.48
PA6-3.40/PA66	89.37	0.053	315.90
PA6-2.40/TPAE	272.76	0.068	406.71
T400	69.43	0.040	237.81

2.5 Dyeing performance analysis of PA-based side-by-side bicomponent elastic fabrics

Dyeing performance is an important indicator of the fabric performance, especially the dyeing uniformity. Therefore, the fabric is dyed with an acid dye to evaluate the dyeing performance of the PA-based side-by-side bicomponent elastic fabrics. The dyed fabrics are shown in Fig. 10 and the dye uptakes are shown in Table 4. Except that PA6-2.40/PA6-3.40 fabric is slightly undyed, most fabrics show good dyeing uniformity, which indicating that although the side-by-side structure could affect the dyeing uniformity of the fabrics, the fabrics still maintain good dyeing properties for clothing.

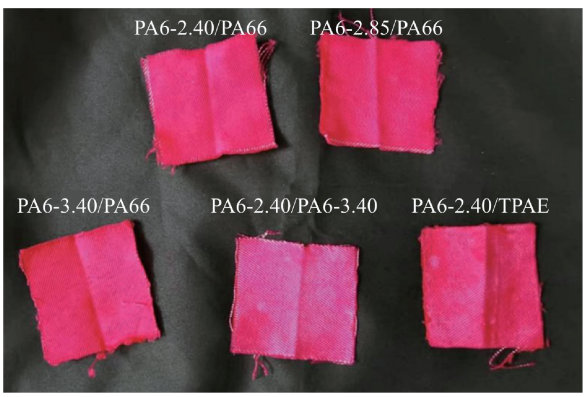

Fig. 10 Dyed PA-based side-by-side bicomponent elastic fabrics

3 Conclusions

In this study, PA-based side-by-side bicomponent elastic fibers were prepared by the melt spinning method using different types of PAs, and the effects of the cross-section shape and unbalanced stresses on the crimp formability were systematically investigated. For the same polymer, the formation of a dumbbell cross-section cannot be stabilized due to rapid mixing between the components. For different polymers, the difference in thermal shrinkage determines the crimp effect of the fibers. The dumbbell cross-sectional shape and the existence of thermal shrinkage differences between components are necessary conditions for the formation of the crimp structure. The PA-based side-by-side bicomponent elastic fibers with intrinsic elastomer TPAE and PA6 as components have the best crimp properties. And the crimp ratio is 7.23%, which is higher than that of commercial T400 fibers. The excellent crimp performance of PA6/TPAE comes from the asymmetric distribution of the stress along the radial direction during the cooling process, which is caused by the difference in thermal shrinkage between PA6 and TPAE. At the same time, the movement of the segments in the amorphous area during the wet-heat treatment causes the component of the fiber to thermally shrink to varying degrees, thereby further developing the fiber crimp structure. The crimp ratio of PA6-2.40/TPAE increases from 7.23% to 33.08% after wet-heat treatment. Moreover, the fabrics made of the PA-based side-by-side bicomponent elastic fibers have better moisture and air permeability than those made of the commercial T400 fibers. The PA6-2.40/TPAE fabric exhibits an air permeability of 272.76 mm/s and a water vapor transmission rate of 406.71 g/(m^2·h), which are 3.93 and 1.71 times those of T400 fabric, respectively. It means that the fabrics made of the PA-based side-by-side bicomponent elastic fibers have better wearing comfort and can meet the higher comfort requirements for elastic products.

References

[1] HU J L, LU J, ZHU Y. New developments in elastic fibers[J]. *Polymer Reviews*, 2008, 48(2): 275-301.

[2] SONG X Y. Elasticity, auxiliary, dyeing and finishing of elastic fiber textiles [J]. *Textile Auxiliaries*, 2011, 28(3): 1-14. (in Chinese)

[3] WANG L L, DONG X, ZHU P, et al. High elasticity and corresponding microstructure origin of novel long chain poly(amide-block-ether) filament fibers[J]. *European Polymer Journal*, 2017, 90: 171-182.

[4] BAI Y F, ZHENG L, DING H, et al. Design of sleeveless tight-fitting sensing clothing based on ANSYS workbench [J]. *Journal of Donghua University (English Edition)*, 2024, 41(1): 8-14.

[5] XIAO H Y, XIAO H, SHI M W, et al. The mechanical property and application of three kinds of elastic fibers[J]. *Synthetic Fiber in China*, 2008, 37(12): 24-28. (in Chinese)

[6] HICKS E M Jr, ULTEE A J, DROUGAS J. Spandex elastic fibers[J]. *Science*, 1965, 147(3656): 373-379.

[7] CASEY P, CHEN H Y, POON B, et al. Polyolefin based crosslinked elastic fiber: a technical review of DOW XLA™ elastic fiber technology[J]. *Polymer Reviews*, 2008, 48(2): 302-316.

[8] LIU H K, WANG T, YAN Z S, et al. Elastic bio-based polyurethane nanofibrous membrane with robust waterproof and breathable properties [J]. *Journal of Donghua University (English Edition)*, 2023, 40(3): 237-246.

[9] SUN J, ZHANG W W, LI F Y, et al. Effect of heat treatment with alternating tension on microstructure and elastic recovery of poly(trimethylene terephthalate) fibers[J]. *Polymers for Advanced Technologies*, 2022, 33(8): 2425-2433.

[10] TAE H O. Melt spinning and drawing process of PET side-by-side bicomponent fibers[J]. *Journal of Applied Polymer Science*, 2006, 101(3): 1362-1367.

[11] ZHU S F, MENG X, YAN X, et al. Evidence for bicomponent fibers: a review [J]. *e-Polymers*, 2021, 21(1): 636-653.
[12] CHIEN A T, GULGUNJE P V, CHAE H G, et al. Functional polymer-polymer/carbon nanotube bi-component fibers [J]. *Polymer*, 2013, 54(22): 6210-6217.
[13] YU J C, LI X Y, JI H, et al. Evaluation of the crimp formability of side-by-side PLA/PTT bicomponent fibers [J]. *Textile Research Journal*, 2021, 91(15/16): 1865-1875.
[14] LIAO H, ZHANG Y, ZHANG Y M, et al. Evolution of interfacial formation and configuration control of bicomponent fiber during full spinning process [J]. *Textile Research Journal*, 2023, 93(3/4): 971-982.
[15] YANG B, WANG R, DONG Z F, et al. Three-dimensional crimped biodegradable poly (lactic acid) fibers prepared via melt spinning and controlled structural reorganization [J]. *RSC Advances*, 2020, 10(70): 42890-42896.
[16] YU J C, CHEN K, JI H, et al. Facile and large-scale fabrication of self-crimping elastic fibers for large strain sensors [J]. *Chinese Journal of Polymer Science*, 2021, 39(7): 914-924.
[17] LUO J, XU G B, WANG F M. External configuration and crimp parameters of PTT (polytrimethylene terephthalate)/PET (polyethylene terephthalate) conjugated fiber [J]. *Fibers and Polymers*, 2009, 10(4): 508-512.
[18] PRAHSARN C, KLINSUKHON W, ROUNGPAISAN N, et al. Self-crimped bicomponent fibers containing polypropylene/ethylene octene copolymer [J]. *Materials Letters*, 2013, 91: 232-234.
[19] OH T H. Effects of spinning and drawing conditions on the crimp contraction of side-by-side poly (trimethylene terephthalate) bicomponent fibers [J]. *Journal of Applied Polymer Science*, 2006, 102(2): 1322-1327.
[20] LUO J, WANG F M, XU B G. Factors affecting crimp configuration of PTT/PET bi-component filaments [J]. *Textile Research Journal*, 2011, 81(5): 538-544.
[21] MARCHILDON K. Polyamides-still strong after seventy years [J]. *Macromolecular Reaction Engineering*, 2011, 5(1): 22-54.
[22] ZHANG S M, ZHANG J C, TANG L, et al. A novel synthetic strategy for preparing polyamide 6 (PA6)-based polymer with transesterification [J]. *Polymers*, 2019, 11(6): 978.
[23] ZHANG S M, WU Y H, JI P, et al. Sustainable production of polyamide 6 fibers: direct melt spinning and efficient reuse of residual oligomers during polymerization [J]. *ACS Sustainable Chemistry & Engineering*, 2023, 11(9): 3789-3800.
[24] CHOI Y B, KIM S Y. Effects of interface on the dynamic mechanical properties of PET/nylon 6 bicomponent fibers [J]. *Journal of Applied Polymer Science*, 1999, 74(8): 2083-2093.
[25] AYAD E, CAYLA A, RAULT F, et al. Influence of rheological and thermal properties of polymers during melt spinning on bicomponent fiber morphology [J]. *Journal of Materials Engineering and Performance*, 2016, 25(8): 3296-3302.
[26] GONG S, ZHAO S K, CHEN X Y, et al. Thermoplastic polyamide elastomers: synthesis, structures/properties, and applications [J]. *Macromolecular Materials and Engineering*, 2021, 306(12): 2100568.
[27] FU P, ZHANG J H, ZHANG Y C, et al. Shape memory thermoplastic polyamide elastomer based on PA1212 [J]. *Macromolecular Materials and Engineering*, 2023, 308(4): 2200547.
[28] FU X B, ZHANG T, YANG J C, et al. Structures and properties of newly synthesized semi-aromatic polyamide thermoplastic elastomers [J]. *Polymer Chemistry*, 2022, 13(34): 4980-4991.
[29] YU Y C, JO W H. Segmented block copolyetheramides based on nylon 6 and polyoxypropylene. I. Synthesis and characterization [J]. *Journal of Applied Polymer Science*, 1994, 54(5): 585-591.
[30] YU Y C, JO W H. Segmented block copolyetheramides based on nylon 6 and polyoxypropylene. II. Structure and properties [J]. *Journal of Applied Polymer Science*, 1995, 56(8): 895-904.
[31] WANG Z, LIN N, KANG H L, et al. Isodimorphism in polyamide 56/polyamide 66 blends with controllable thermal and mechanical properties [J]. *ACS Applied Polymer Materials*, 2022, 4(12): 9407-9416.
[32] WANG Z, LIN N, KANG H L, et al. Miscibility, crystallization and properties of bio-based polyamide 56/polyamide 6 blends [J]. *Polymer*, 2023, 265: 125603.
[33] YUAN R C, FAN S, WU D Q, et al. Facile synthesis of polyamide 6 (PA6)-based thermoplastic elastomers with a well-defined microphase separation structure by melt polymerization [J]. *Polymer Chemistry*, 2018, 9(11): 1327-1336.
[34] RWEI S P, LIN Y T, SU Y Y. Study of self-crimp polyester fibers [J]. *Polymer Engineering & Science*, 2005, 45(6): 838-845.
[35] YANG H J, KIM Y K, SON J A, et al. Preparation of modified polylactic acid fiber containing anti-hydrolysis agents [J]. *Journal of Applied Polymer Science*, 2023, 140(38):

e54436.
[36] CHEN J, GONG C H, YANG C, et al. Flexible preparation of polyamide-6 based thermoplastic elastomers via amide exchange[J]. *Journal of Materials Science*, 2021, 56(20): 12018-12029.
[37] LUO K M, LIU J X, ABBAY K, et al. The relationships between the structure and properties of PA56 and PA66 and their fibers [J]. *Polymers*, 2023, 15(13): 2877.
[38] ZHANG S M, WU Y H, YANG H B, et al. Preparing cationic dyeable polyamide 6 filaments by combining the masterbatch technique with melt copolymerization[J]. *Textile Research Journal*, 2022, 92(3/4): 511-524.
[39] HE Z L, ZHOU G H, BYUN J H, et al. Highly stretchable multi-walled carbon nanotube/thermoplastic polyurethane composite fibers for ultrasensitive, wearable strain sensors [J]. *Nanoscale*, 2019, 11(13): 5884-5890.
[40] ZHANG S M, FAN X S, XU C C, et al. An inherently flame-retardant polyamide 6 containing a phosphorus group prepared by transesterification polymerization [J]. *Polymer*, 2020, 207: 122890.
[41] JIANG J, TANG Q Y, PAN X, et al. Facile synthesis of thermoplastic polyamide elastomers based on amorphous polyetheramine with damping performance[J]. *Polymers*, 2021, 13(16): 2645.
[42] JIANG J, TANG Q Y, PAN X, et al. Structure and morphology of thermoplastic polyamide elastomer based on long-chain polyamide 1212 and renewable poly(trimethylene glycol)[J]. *Industrial & Engineering Chemistry Research*, 2020, 59(39): 17502-17512.

自卷曲聚酰胺基并列复合弹性纤维的制备及性能研究

吴宇豪[1], 郎嘉瑞[1], 张圣明[1], 刘　津[1], 王朝生[1*], 王华平[1], 吉　鹏[2*]
1. 东华大学 材料科学与工程学院, 纤维材料改性国家重点实验室, 上海 201620
2. 东华大学 纺织科技创新中心, 上海 201620

摘　要: 并列双组分纤维具有弹簧般的三维螺旋卷曲结构, 被广泛应用于弹性织物。不同聚合物之间的热收缩率差异会在冷却过程中产生不平衡应力, 可以利用这种不平衡应力通过纺丝设计制备自然卷曲纤维。该工作选择不同类型的聚酰胺（polyamide, PA), 采用熔融纺丝法制备并列型 PA 双组分弹性纤维, 并研究了 PA 双组分弹性纤维的结构发展和性能。同时, 具有本征弹性的热塑性聚酰胺弹性体（thermoplastic polyamide elastomer, TPAE）被用作对比材料。TPAE 分子链中 PA 链段和聚醚链段的嵌段结构是提供热收缩差异和形成良好界面结构的关键。结果显示, PA6/TPAE 双组分弹性纤维的卷曲率为 7.23%, 优于商品化的 T400 纤维（聚对苯二甲酸丙二醇酯/聚对苯二甲酸乙二醇酯双组分纤维）（6.72%)。PA6/TPAE 双组分弹性纤维优异的卷曲性能来源于冷却过程中沿纤维径向产生的不对称应力, 这是由 PA6 和 TPAE 的热收缩率差异造成的。此外, 通过湿热处理扩大收缩应力, 可以改善 PA 双组分弹性纤维的卷曲成型性。PA6/TPAE 双组分弹性纤维经 100 ℃处理后卷曲率达到最大值 33.08%。同时, PA6/TPAE 双组分弹性纤维制成的织物具有优异的透气透湿性能, 透气率为 272.76 mm/s, 透湿率为 406.71 g/(m^2 · h)。

关键词: 双组分纤维; 聚酰胺（PA）纤维; 自卷曲; 卷曲成型性; 熔融纺丝